crystals

MDPI

Review

Lithium Tetraborate as a Neutron Scintillation Detector: A Review

Elena Echeverria [1,*], John McClory [2], Lauren Samson [3,4], Katherine Shene [3], Juan A. Colón Santana [5], Yaroslav Burak [6], Volodymyr Adamiv [6], Ihor Teslyuk [6], Lu Wang [7], Wai-Ning Mei [8], Kyle A. Nelson [9], Douglas S. McGregor [9], Peter A. Dowben [10,*], Carolina C. Ilie [3,*], James Petrosky [2,*] and Archit Dhingra [11,*]

1 Department of Physics, Oklahoma State University, 145 Physical Sciences Bldg., Rm 546, Stillwater, OK 74078, USA
2 Department of Engineering Physics, Air Force Institute of Technology, 2950 Hobson Way, Wright-Patterson AFB, OH 45433, USA; john.mcclory@afit.edu
3 Physics Department, SUNY Oswego, 254 Shineman Center, Oswego, NY 13126, USA; kshene@oswego.edu (K.S.)
4 Department of Physics, University at Buffalo, 239 Fronczak Hall, Buffalo, NY 14260-1500, USA
5 Department of Physics, Aurora University, 347 S. Gladstone Ave., Aurora, IL 60506-4892, USA; jsantana@aurora.edu
6 Institute of Physical Optics, 23 Dragomanov Str., 79-005 Lviv, Ukraine; burak@ifo.lviv.ua (Y.B.); adamiv@ifo.lviv.ua (V.A.); teslyuk@ifo.lviv.ua (I.T.)
7 CAS Key Lab of Materials for Energy Conversion, University of Science and Technology of China, Jinzhai Road 96, Hefei 230026, Anhui Province, China; lukewl@ustc.edu.cn
8 Department of Physics, University of Nebraska–Omaha, Omaha, NE 68182, USA; physmei@unomaha.edu
9 S.M.A.R.T. Laboratory, Mechanical and Nuclear Engineering Department, Kansas State University, Manhattan, KS 66506, USA; nuclearengg@gmail.com (K.A.N.); mcgregor@ksu.edu (D.S.M.)
10 Department of Physics and Astronomy, University of Nebraska-Lincoln, 855 North 16th Street, Lincoln, NE 68588, USA
11 Institut de Ciència dels Materials de la Universitat de València (ICMUV), University of Valencia, Carrer del Catedrátic José Beltrán Martinez, 2, 46980 Paterna, Valencia, Spain
* Correspondence: eme54@cornell.edu (E.E.); pdowben@unl.edu (P.A.D.); carolina.ilie@oswego.edu (C.C.I.); jpetrosky@thinkdeterrence.com (J.P.); archit.dhingra@uv.es (A.D.)

Citation: Echeverria, E.; McClory, J.; Samson, L.; Shene, K.; Colón Santana, J.A.; Burak, Y.; Adamiv, V.; Teslyuk, I.; Wang, L.; Mei, W.-N.; et al. Lithium Tetraborate as a Neutron Scintillation Detector: A Review. *Crystals* **2024**, *14*, 61. https://doi.org/10.3390/cryst14010061

Academic Editors: Yutaka Fujimoto and Zongyou Yin

Received: 24 November 2023
Revised: 11 December 2023
Accepted: 28 December 2023
Published: 31 December 2023

Abstract: The electronic structure and translucent nature of lithium tetraborate ($Li_2B_4O_7$) render it promising as a scintillator medium for neutron detection applications. The inherently large neutron capture cross-section due to ^{10}B and ^{6}Li isotopes and the ease with which $Li_2B_4O_7$ can be enriched with these isotopes, combined with the facile inclusion of rare earth dopants (occupying the Li^+ sites), are expected to improve the luminescent properties, as well as the neutron detection efficiency, of $Li_2B_4O_7$. The electronic structure of both doped and undoped $Li_2B_4O_7$ were explored, using photoemission and inverse photoemission spectroscopies, optical measurements, and theoretical computational studies such as density functional theory. The scintillation properties are further enhanced because of the wide bandgap, making $Li_2B_4O_7$ extremely translucent, so that capturing the neutron scintillation output is neither hindered nor diminished. Therefore, in this review, demonstrations of the possible amplification of neutron capture efficiencies, courtesy of rare-earth dopants, along with insights into a significantly large charge production (associated with neutron capture), are presented.

Keywords: lithium tetraborate; neutron detectors; rare earth dopants; neutron scintillation detectors

1. Introduction

Neutron detection is an inherent component of neutron radiation dosimetry, cross-border interdiction of fissile materials [1,2], nuclear reactor fuel and nuclear safety management [3,4], nonproliferation, nuclear stockpile monitoring, and nuclear medicine [5]. These particles are uncharged, which means that they do not provide a direct electronic signal, and they do not readily interact with most matter. In short, when compared to detection of other forms of radiation, neutron detection is nothing short of an ordeal. Therefore, when, in a Senate hearing, Dr. Robert J. Oppenheimer was asked what instrument he would use to

detect an atomic bomb, his answer was "a screwdriver", implying one would have to open every container to detect fissile materials because radiation emanations were extremely small [6].

Due to abovementioned reasons, practical neutron detection methods rely on indirect measurements based upon an initial neutron interaction producing a secondary species (conversion) that is readily measurable due to its effect on electronic and/or optical properties [7]. Neutron detectors are, therefore, divided into electronic (gas-filled or semiconductor devices, where ionization leads to an induced current or voltage pulse) or scintillation (absorption of radiation followed by luminescence in the material) detectors. However, the process of selecting just the right kind of materials to manufacture reliable neutron detectors faces a colossal challenge of circumventing the background radiation. To elaborate further, background γ-ray emissions, either from natural terrestrial sources or from the γ-ray emitters associated with the neutron source, can mask the secondary ionization or excitation signal from a neutron detector as well. Thus, many applications seek materials made of the lighter elements to remove or reduce the signals that might arise from associated X-ray and γ radiation, often referred to as being "γ-ray blind" [7], meaning that a very high neutron-to-gamma-ray detection ratio is sought [8]. Currently, there exist six kinds of materials used as scintillators: organic crystals, organic liquids, plastics, inorganic crystals, gases, and glasses. Among these materials, crystal, glass, and gas scintillators are often used for neutron detection; however, gases are less sensitive to β (beta) and γ (gamma) radiation, while the background from γ rays is generally higher for solids and liquids due to the higher atomic density. For thermal neutrons in particular, detectors with a high concentration of ^{6}Li are employed because they enhance the scintillation sensitivity [9], which is why lithium tetraborate ($Li_2B_4O_7$) has been touted to be a highly efficient material for applications in scintillation neutron detectors [10–13].

In this review article, the crystal and optical properties of the lithium tetraborate ($Li_2B_4O_7$) are described. The optical properties and photoemission characteristics are discussed in detail to understand the advantage of using this material as a scintillator neutron detector. The most important results on the rare earth (RE) doping of this material and how this doping enhances the scintillation characteristics are also presented. Therefore, new research directions on scintillation efficiency and transparency can be identified through this review article. This information is critical to finally design and manufacture high-efficiency and low-cost $Li_2B_4O_7$-based neutron scintillation detectors.

2. Lithium Tetraborate-Based Scintillation Detectors

Lithium tetraborate, usually known for its pyroelectric and piezoelectric properties [14–16], is a complex tetragonal crystal with 104 atoms per unit cell (see Figure 1a), with dimensions a = b = 9.470 Å and c = 10.290 Å and a space group of $I4_1cd$ [17]. It has a characteristic wide electronic bandgap of ~8.9 to 10.1 eV [18], a large capability for thermal neutron capture, and high resistance to radiation damage. $Li_2B_4O_7$ is also known to possess the best scintillation parameters among all the lithium borates [11,12,19,20], and multiple examples of experimental evidence advocating for the use of $Li_2B_4O_7$ as a scintillator have existed for quite some time now [12].

Work by Zadneprovski et al. [11] confirmed that undoped $Li_2B_4O_7$ is in fact γ blind, that is to say, largely insensitive to γ-ray radiation due to low γ-ray cross-sections, which is consistent with the fact that the primary elemental constituents of $Li_2B_4O_7$ all have very low Z (i.e., atomic number) values. Since $Li_2B_4O_7$ growth requires little post-material fabrication processing, scintillation detectors based on $Li_2B_4O_7$ hold promise for an inexpensive and efficient detection system. Moreover, lightweight $Li_2B_4O_7$ sheets can be combined with multiple scintillation–photomultiplier tubes into a single PIN diode (or photon sensor), so they can be scaled to large areas with little need for increased power or loss of detection area due to the need for pixelation and concomitant device connections, as would be the case in a solid-state device. Detectors based on $Li_2B_4O_7$ can therefore be made thick enough to provide the necessary neutron moderation within the detector medium,

leading to higher absolute efficiency. Lastly, $Li_2B_4O_7$ is fairly immune to terrestrial-level temperature changes and unaffected by moisture and corrosion, making it well-suited for harsh environmental applications.

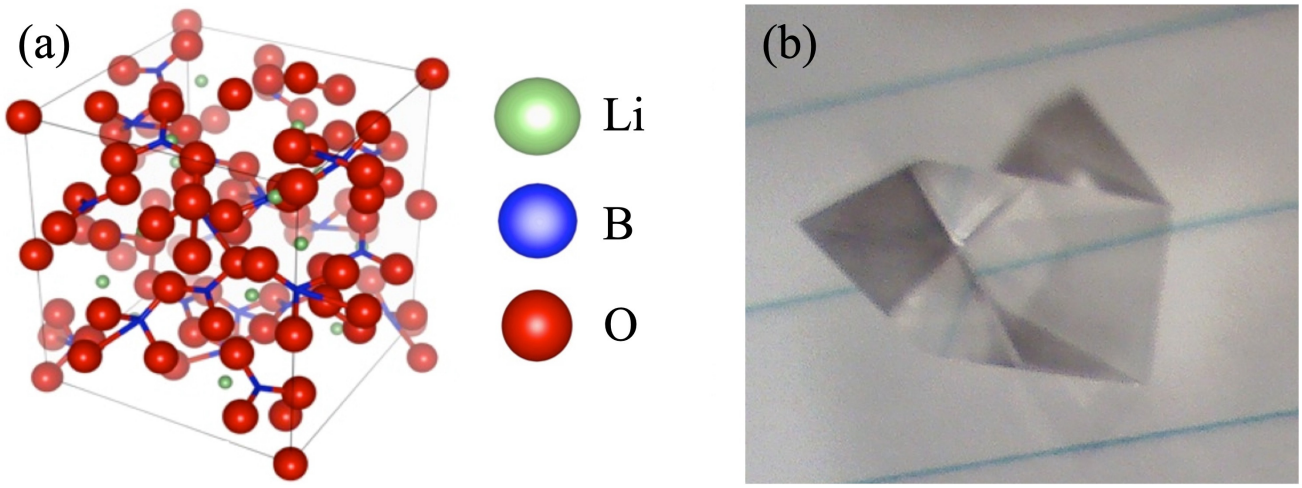

Figure 1. (**a**) The structure of lithium tetraborate ($Li_2B_4O_7$) and (**b**) a lithium tetraborate single crystal showing excellent translucence.

In terms of the physics of operation, the advantage of using $Li_2B_4O_7$ as a neutron detection medium arises from the high thermal neutron capture cross-section inherent in the nuclear isotopes of $^{10}_{5}B$ (σ_B = 3935 barns) and $^{6}_{3}Li$ (σ_{Li} = 940 barns). Natural B consists of ~20% of ^{10}B, and natural Li consists of ~6% of ^{6}Li. Luminescence is generated by electron–hole pair creation and annihilation resulting from the energetic daughter products of ^{10}B [9] and ^{6}Li [10] capture reactions, as shown below:

$^{10}B + n \rightarrow {}^{7}Li\ (0.84\ MeV) + {}^{4}He\ (1.47\ MeV) + \gamma\ (0.48\ MeV)\ (94\%)$

$^{10}B + n \rightarrow {}^{7}Li\ (1.015\ MeV) + {}^{4}He\ (1.78\ MeV)\ (6\%)$

$^{6}Li + n \rightarrow {}^{3}H + {}^{4}He + (4.8\ MeV)$

In order to improve the neutron interaction probability, $Li_2B_4O_7$ can be formed using Li and B enriched with ^{6}Li and ^{10}B, respectively [10], thus increasing the thermal neutron capture cross-section. Both isotopes can be enriched using standard isotopic separation techniques. And even though standard isotopic separation techniques can be applied to enhance the enrichment of both the isotopes, usually Li is more widely used than B because its neutron capture reaction products have higher energy and lead to greater light output. Both the ^{6}Li and ^{10}B daughter fragments have significant kinetic energies, which, in turn, can lead to the creation of electron–hole pairs. The subsequent electron–hole pairs can then recombine to create light, but detection of the scintillation is more easily achieved if the light is in the visible range and the scintillation output is coupled with the photomultiplier or photodiode detector. Obviously, the light has to reach the detector, so a scintillator material that is close to transparent is ideal. This means that the optical properties and bandgap matter. But there are trade-offs, as discussed below. For example, a large bandgap may ensure a more translucent material but lead to the creation of fewer electron–hole pairs along the charge tracks left by the ^{6}Li and ^{10}B daughter fragments.

Single-crystal $Li_2B_4O_7$, in its pure form, exhibits luminescence, but the scintillation efficiency is insufficient for practical neutron detection applications [21]. Another major drawback to using $Li_2B_4O_7$ as a scintillation detector is that, like many glass-based materials, it is sensitive to electron (β), proton, and α radiation. Although it is possible to use a pulse height discrimination technique to separate ^{6}Li or ^{10}B neutron capture events from other events, the response time is on the order of 10 ns, and the light output is low, typically approximately 30% of that of anthracene [9]. In order to compensate for this disadvantage, the light output must be maximized to produce an adequate neutron capture

scintillation response, obtained by select doping of the material. Fortunately, $Li_2B_4O_7$ readily accepts the incorporation of dopants such as Cu and Ag, as well as rare earth elements, such as Yb [11,22], Ce [11], Nd [19,21], Sm [11], Eu [11,23], Gd [19], Tb [11], Er [19], and Tm [11,24], that enhance the luminescence by increasing recombination sites and adding luminescence lines [11,22–28], thus increasing the luminescent efficiency. Rare earth elements are especially useful, as they exhibit sharp luminescence originating from their intra-4f electronic transitions [22–26,29–50].

The partly filled 4f orbitals of the rare earth elements in conjunction with a filled 5s and 5p subshell provide enough shielding from the crystal field (electric field exerted by neighboring atoms) so that the energy levels of the rare earth ion closely resemble those of the free ions when incorporated into the $Li_2B_4O_7$. This is evident from detailed electronic structure calculations of various rare earth dopants substitutionally placed in the $Li_2B_4O_7$ lattice [25]. This property greatly increases luminescence efficiencies, i.e., signal above background, with the addition of small amounts of rare earths. Thus, the light output, generated as a consequence of neutron capture, is more readily detected in a photodetector and more easily distinguished from background. The doped $Li_2B_4O_7$ results in a better linear dose response as compared to common thermoluminescent dosimeter materials (e.g., LiF), making it an attractive material for dosimetry applications [20,25,28,51]. Although many elements have been used for doping $Li_2B_4O_7$, only cerium-activated lithium or borosilicate glass scintillators are well established and widely used as thermal (slow) neutron detectors [9,11,52–55]. And if the goal is to improve the sensitivity of $Li_2B_4O_7$, it can be achieved by doping it with Ag [28]; in addition, combining the Ag-doped $Li_2B_4O_7$ with solar-blind photomultiplier can also lead to a high signal-to-noise ratio [28].

3. The Optical Characteristics of $Li_2B_4O_7$

Owing to the wide electronic bandgap (~8.9 to 10.1 eV), as seen in the combined photoemission and inverse photoemission measurements [15,18], $Li_2B_4O_7$ single crystals are transparent across a wide range of 165–6000 nm, and the fundamental absorption maximum is located at about 133 nm [15]. In nature, $Li_2B_4O_7$ occurs as a clear, colorless mineral, as inclusions of diomignite in pegmatite, and it can be easily manufactured into crystals or glasses. As mentioned before, it can be fabricated into large sheets, using readily available manufacturing techniques, so the assembly of large area detector arrays is possible, and costs can be relatively low [51] because specialized materials processing is not required. Pure $Li_2B_4O_7$ glasses, on the other hand, typically present high transparency in the range of 300–2600 nm, with three low-intensity emission bands centered at 402 nm, 520 nm, and 728 nm [11]. Regardless of whether it is a $Li_2B_4O_7$ single crystal or a pure $Li_2B_4O_7$ glass, the addition of dopants can be expected to alter their respective luminescence spectrum.

Figure 2 presents the transmission spectra of both undoped and doped single crystals of $Li_2B_4O_7$. In this figure, signatures of an apparent trade-off between luminescence and transparency, as an increase in luminescence comes at the cost of transparency and efficiency of light collection, are observed. Doping $Li_2B_4O_7$ single crystals with Ag gives birth to new absorption bands at 174 nm and 205 nm (indicated by the arrows in the figure), whereas both undoped and Cu-doped $Li_2B_4O_7$ crystals present a broad low-intensity band [51].

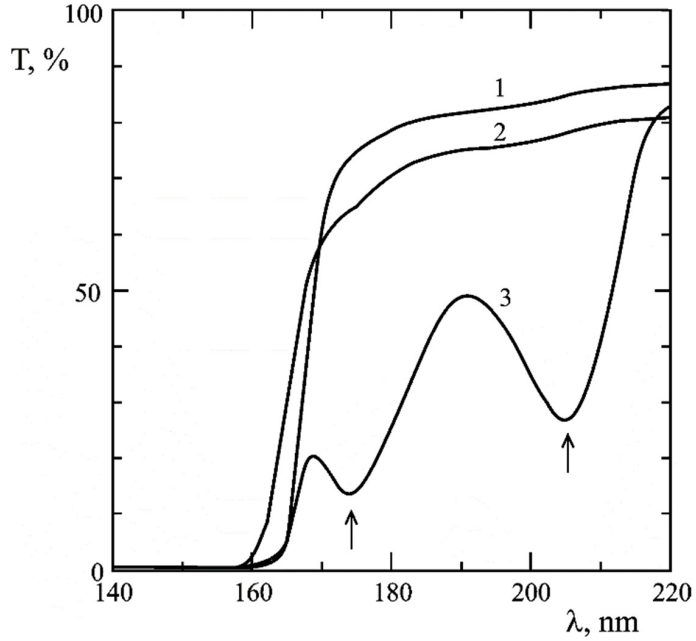

Figure 2. Room-temperature transmission spectra of $Li_2B_4O_7$ single crystals: 1—undoped; 2—Cu doped; 3—Ag doped. Adapted from [56].

Figure 3 presents the electronic band configuration of $Li_2B_4O_7$ obtained from photoemission spectroscopy (PES) and inverse photoemission spectroscopy (IPES). The spectra reveal several sub-band transitions. The valence band has a high-intensity (or high electron density) primary peak in photoemission (below the Fermi level (E_F)), and the strong feature above E_F, observed in inverse photoemission, denotes the conduction band edge. A detailed analysis of the structures shown in Figure 3 unveils that the top of the valence band in a $Li_2B_4O_7$ single crystal is mainly occupied by just boron–oxygen groups, while the bottom of its conduction band includes orbital contributions from lithium as well [15,57]. The energy interval between the two strong spectral features in Figure 3, one each in photoemission and inverse photoemission, represent the ground-state bandgap. From these measurements [15,18] on a $Li_2B_4O_7$(100) crystal, the ground-state bandgap is found to be 9.8 ± 0.5 eV, falling right in the range between 8.9 ± 0.5 eV and 10.1 ± 0.5 eV [15,18,56,58,59], which is somewhat in line with theoretical expectations [57]. These measured values for the ground-state bandgap are higher than the previously measured values of the optical gap (E_g (opt) = 7.4 eV) extrapolated from the absorption plot [15,56], but they are closer to the theoretical ground-state bandgap. This means that incident photons possessing energy less than the ground-state bandgap, determined from photoemission and inverse photoemission, can still create electron–hole pairs by exciting electrons from the valence band to the conduction band. The creation of carriers will manifest as an increase in the conductivity of the crystal, especially if the carrier mobility and lifetimes are reasonable. Such an increase in the electron population in the conduction band due to optical excitations will, in turn, amplify the photoconductivity of $Li_2B_4O_7$ crystal, while modifying its optical parameters. That is to say, once the $Li_2B_4O_7$ crystal becomes conductive, the complex refractive index, $\widetilde{n} = n(1 + i\chi)$, becomes more relevant to the crystal structure model.

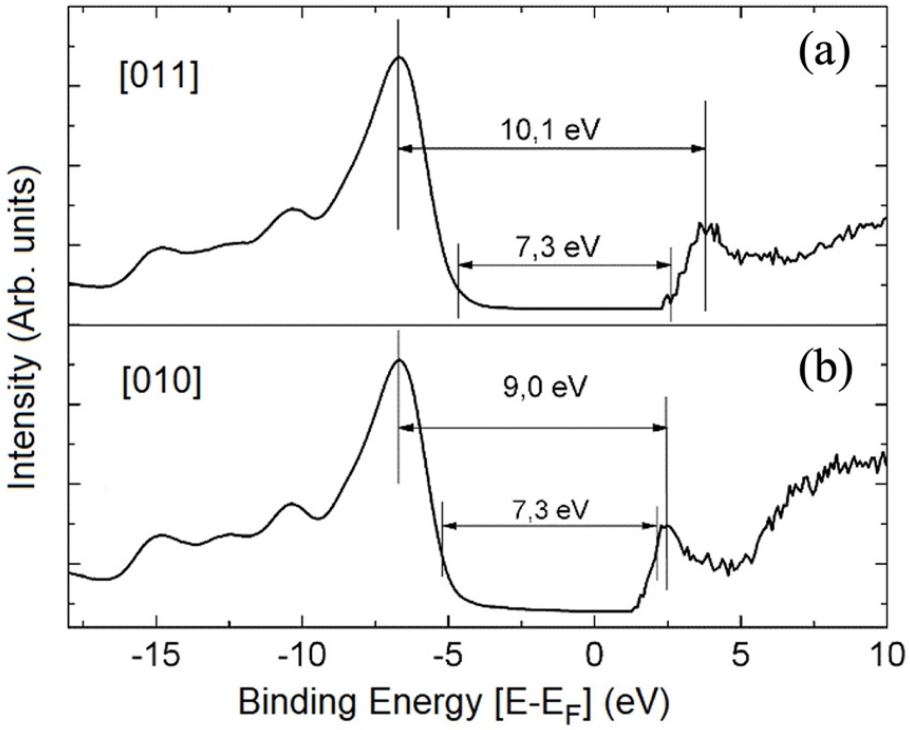

Figure 3. The intensity of the combined experimental photoemission (left) and inverse photoemission (right) data for a Li2B4O7(100) crystal along (a) [011] and (b) [010] as a function of the binding energy E–E_F, where E_F is the Fermi level. Adapted from [18].

The overall dielectric function for all coordinate indices for $Li_2B_4O_7$ can be determined via the crystallographic direction-dependent density functional theory (DFT). However, bandgaps estimated from DFT are subject to error and typically produce an incorrect bandgap that is smaller than the true ground-state bandgap [60–63]. Therefore, the scissor approximation method (SOA) was applied to the real ε_1(E) and imaginary ε_2(E) parts of the dielectric function (shown in Figure 4). In these calculations, the scissor correction error of 1.04 eV is towards the lower end of the range specified by Rasmussen [64] of 1-to-3 eV. This error is small, producing a near-identical approximation to the ground-state bandgap of 7.3 eV that is found using the generalized gradient approximation (GGA), shown in Figure 5. Here, it must be noted that this gap of 7.3 eV is close to the ~7.4 eV gap inferred from optical transmission (Figure 2) and the band edges seen in combined photoemission and inverse photoemission (Figure 3); therefore, the usage of these corrections to DFT appears somewhat reasonable. Figure 6 illustrates the calculated absorption coefficient and refractive index with and without using the scissor approximation averaged over three directions to account for the fact that all crystal faces are not identical in their symmetry.

In addition, with the use of Sellmeier equations, the refractive index of the single lithium tetraborate crystals can be easily verified. The Sellmeier equations applied to the $Li_2B_4O_7$ crystals are as follows [65–67]:

$$n_0^2 = 2.56431 + \frac{0.012337}{\lambda^2 - 0.013013} - 0.019075\lambda^2$$

$$n_0^2 = 2.38651 + \frac{0.010664}{\lambda^2 - 0.012878} - 0.012813\lambda^2$$

The resulting refractive indices are plotted in Figure 7, where n_0^2 and n_e^2 represent the ordinary and extraordinary part of the optical response to the incident light traversing a single lithium tetraborate crystal along the C_4 axis. The curves center on a refractive index of 1.5, which matches the secondary peak seen in Figure 6. In addition, the small differences

in the curves demonstrate nontrivial birefringence, with a bandgap of approximately 7.41 eV to 10.1 eV (with the calculated value being 6.37 eV) indicating an implicit correction of 1.04 eV to 3.73 eV. While 7.3 eV is close to the 7.4–7.5 eV gap determined from optical transmission (Figure 2), the bandgap value of 10.1 eV is close to the ground-state gap of 9–10 eV extrapolated from the combined photoemission and inverse photoemission spectra (Figure 3).

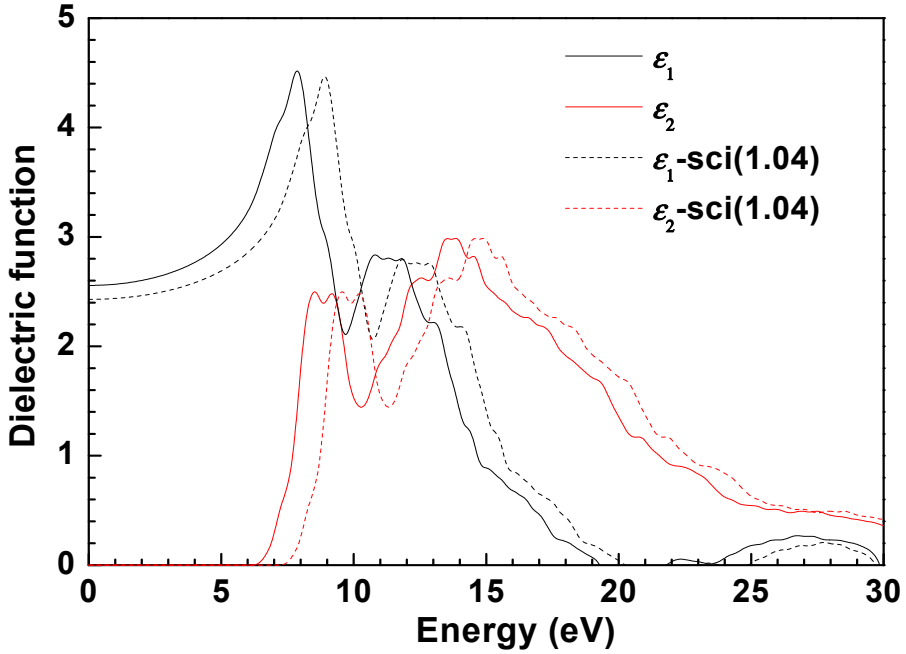

Figure 4. The real ε_1(E) and imaginary ε_2(E) parts of the dielectric constant of a $Li_2B_4O_7$ crystal for the average of the three index directions (solid lines), and then calculated after application of the scissor operator (dashed lines) to correct for the underestimated bandgap that is typical of DFT.

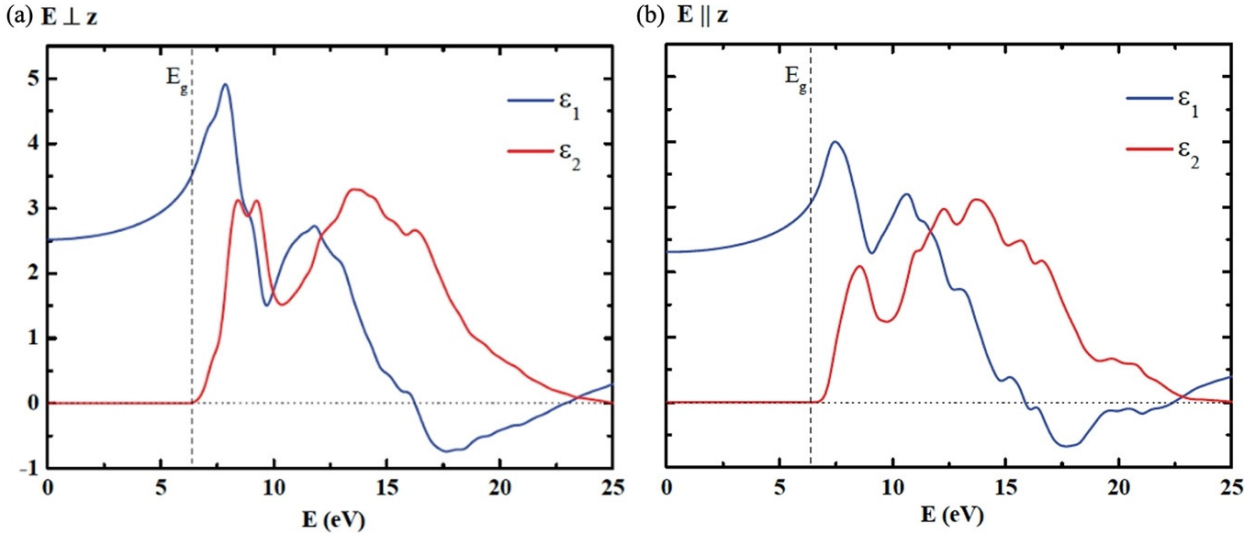

Figure 5. Calculated spectra of real ε_1(E) and imaginary ε_2(E) parts of the dielectric constant of $Li_2B_4O_7$ crystal from DFT with the generalize gradient approximation (GGA). E_g represents the calculated bandgap (6.37 eV). (**a**) Data for incident light **E** perpendicular to the *z*-axis. (**b**) **E** parallel to the *z*-axis.

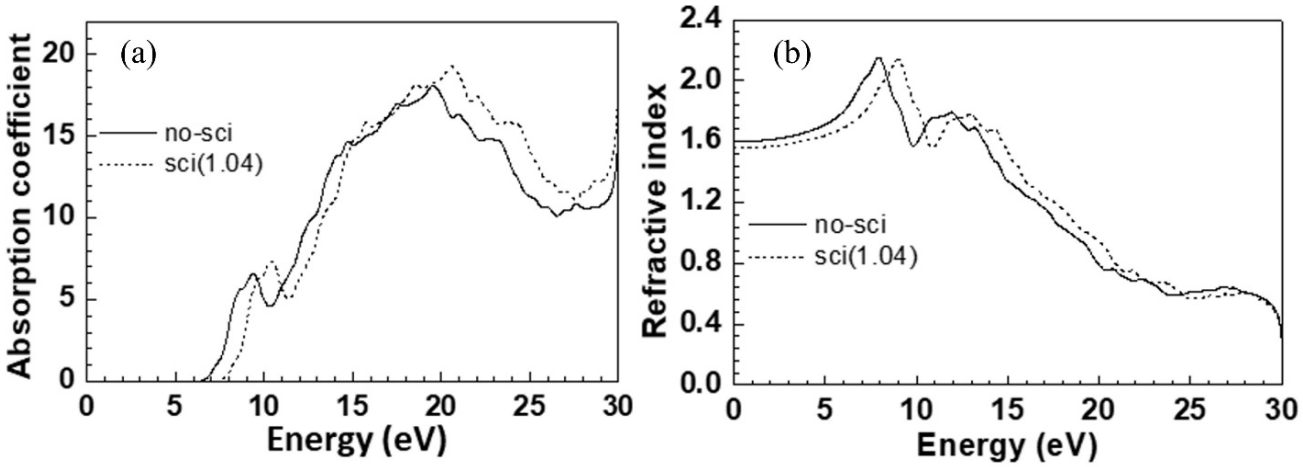

Figure 6. Both (**a**) absorption coefficient and (**b**) refractive index are calculated before (solid line) and after the application of the scissor operator (dashed line) to correct for the underestimated bandgap that is typical for DFT calculations.

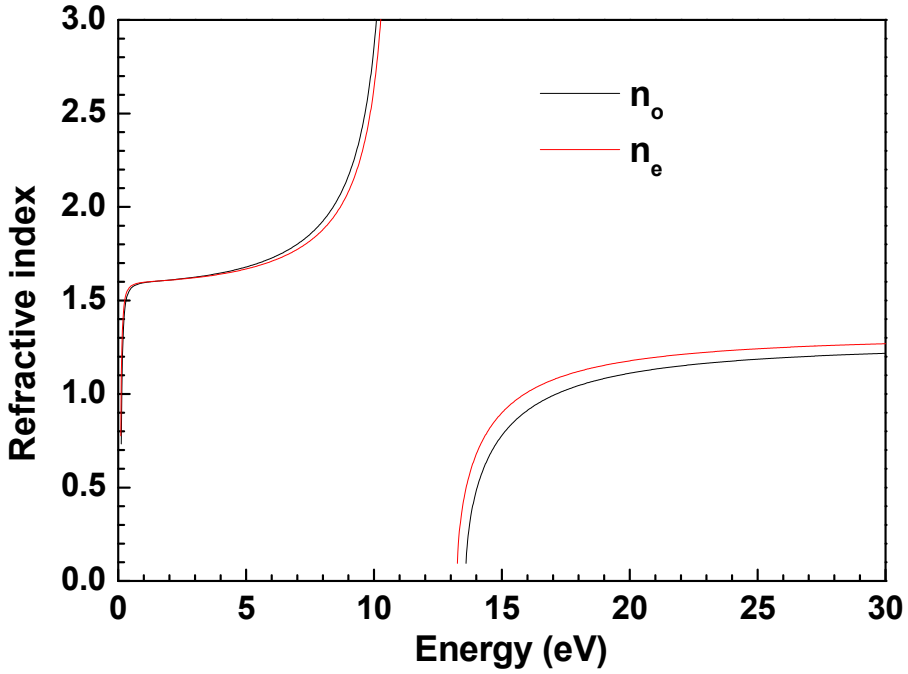

Figure 7. The refractive index as a function of energy of the incident photon.

The fact that structural distortions, particularly at the interface of $Li_2B_4O_7$ single crystals, affect the electron levels in atoms was clearly demonstrated by Wooten et al. [18,58] and the theory of [68]. The influences of imperfections and defects in the lattice of $Li_2B_4O_7$ single crystals are highlighted in Figure 8, which illustrates that the absorption edge for the $Li_2B_4O_7$ glass differs substantially from that of the $Li_2B_4O_7$ single crystal [67]. From this figure, it is evident that the fundamental absorption maximum for borate glass occurs at much longer wavelengths [67], i.e., lower energies, in comparison with that of the $Li_2B_4O_7$ single crystal [58,67,69]. For the $Li_2B_4O_7$ glass, the absorption spectrum shows an indistinct absorption edge, which is common for glassy samples since the crystallographic direction-dependent anisotropic optical properties are expected to be suppressed [70]. The electronic structure of disordered media, which include $Li_2B_4O_7$ glasses, can still be reconciled with the electronic states of $Li_2B_4O_7$ single crystals [19], chiefly because of the similarities in the electron energy density distributions. With this in mind, the long wavelength shift

of the absorption edge of the glass in comparison with single crystals can be explained by blurring the boundary of the electronic density of states. Moreover, the energy band model is still valid here, considering that the direct inter-band transitions are forbidden, with indirect transitions of phonons and excitons occurring through mediation. A detailed discussion regarding such indirect optical transitions is presented elsewhere [71].

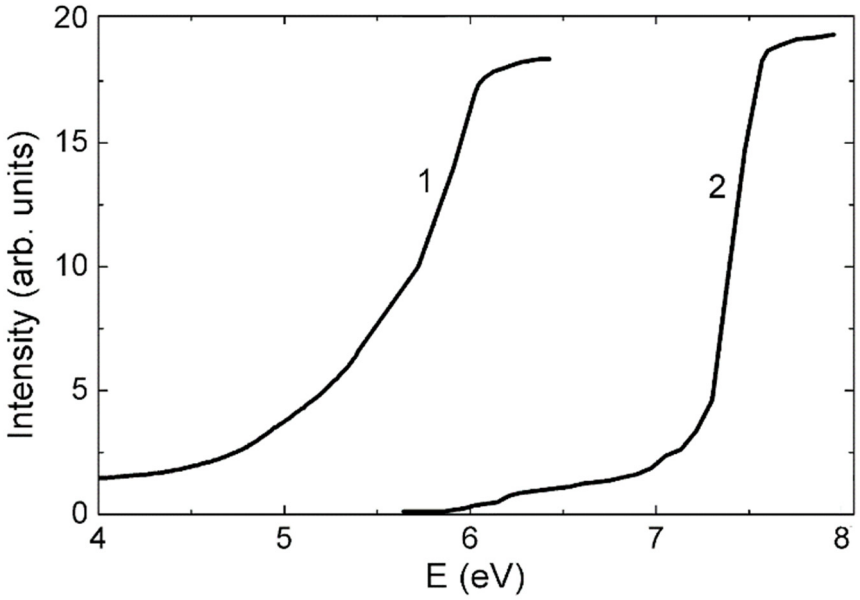

Figure 8. Intrinsic absorption edge of $Li_2B_4O_7$: (1) glass sample and (2) single crystal [67].

4. Factors Affecting Charge Production

As noted above, lithium tetraborate has a ground-state bandgap of roughly 9.8 eV and a measured optical bandgap of 6.7 eV, and this significant bandgap, while improving light transmission, limits the number of electron–hole pairs created by the reaction products resulting from neutron capture. This optical bandgap corresponds to an approximate number of possible charge hole pairs of ~410,000 for the most probable reaction channel of ^{10}B (94%), which has a much higher cross-section than ^{6}Li. This calculation, of course, assumes that all the reaction energy is absorbed. Having said that, for a more accurate calculation, a correction factor to completely account for the production of an electron–hole pair due to the absorption of incoming radiation with an energy above the bandgap must be included. These correction factors have been estimated to be 3.17 [72] and 3.44 [73,74], and employing the correction factor calculated by Klein [72] indicates that a ^{10}B reaction should produce roughly 200,000 charges. Using the same logic for ^{6}Li, approximately 416,000 charges would be produced, but recall that this advantage is reduced since it is known that ^{6}Li has a smaller cross-section and lower elemental concentration. These numbers are, of course, not completely realistic, as they are just the upper limits, as not all of the subsequently created electron–hole pairs will give rise to detectable scintillations. Instead, a neutron capture event near the surface (or an interface) can also result in either an incomplete electron–hole production or Auger-electron production or photoemission. Without defects or a dopant, excitonic decays are capable of producing photons well into the UV, given that the optical gap is 6.7 eV, while the ground-state bandgap is 9.8 eV.

Convincing evidence of electron–hole pair production from neutron irradiation can be collected by considering $Li_2B_4O_7$ as a capacitive detector. The electrical response of a $Li_2B_4O_7$ detector to a neutron fluence is expected to result in a distinctly different pulse count while being irradiated, as compared to the background measurement. A $Li_2B_4O_7$ crystal was irradiated in the radial neutron beam of a TRIGA Mark II nuclear reactor, and the operating bias was increased (or decreased) until a signal was detected. Once the operating biases were fixed upon the detection of a signal, the pulse height spectroscopy

data were recorded, as shown in Figure 9. The shutter to the beam was opened and then closed cyclically between 10-min irradiation measurements and 10-min background measurements, using a multichannel analyzer. These results demonstrate an increase in conductance with neutron capture, consistent with the electron–hole pair creation from the Li and He or ^{3}H and ^{4}He ion tracks. Although counts were observed above the background during irradiation, there are no distinct spectral differences. This outcome indicates that the background electrical noise is likely due to dielectric breakdown or an increase in conductivity due to electron–hole pair creation, much like the expected increase in conductivity due to photocarrier creation discussed above.

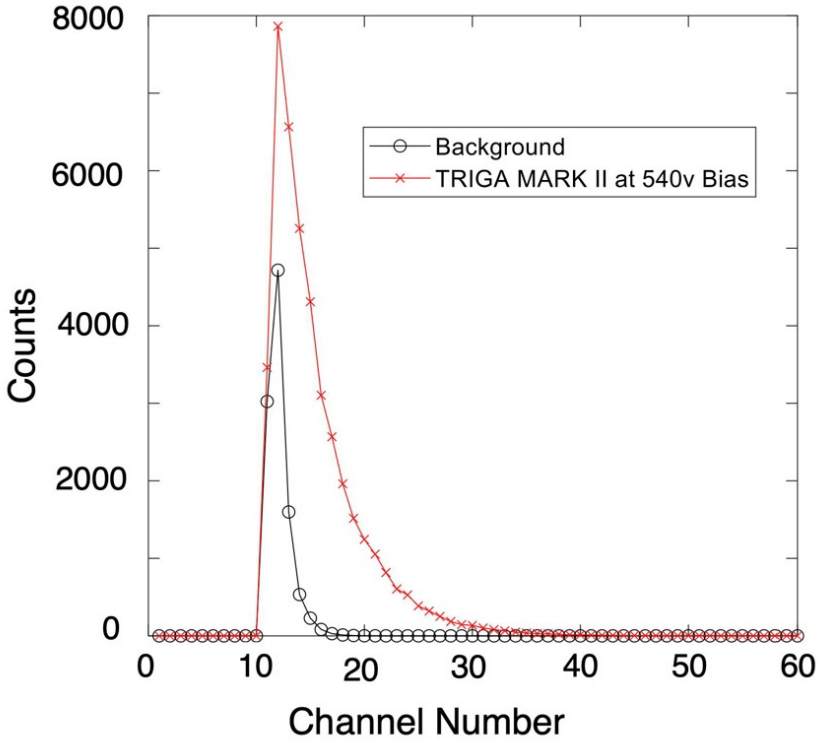

Figure 9. The differential pulse height spectrum obtained for a 10-min count of background- and neutron-irradiated biased $Li_2B_4O_7$ crystal.

5. Factors Affecting Light Production

Based upon the bandgap of $Li_2B_4O_7$, scintillation is expected to produce a photon in the UV energy range. Figure 10 provides the scintillation response of undoped $Li_2B_4O_7$ to α particle radiation from ^{241}Am (Figure 10a), and neutrons plus α particles from a ^{239}Pu source (Figure 10b). In these cases, assessing the interactions with incoming α radiation is particularly important, as α particles are also among the main reaction products of the ^{10}B or ^{6}Li neutron capture reactions. The results shown in Figure 10 confirm that the majority of the light response falls below ~450 nm, which is largely in the UV spectrum (10–400 nm). However, it is desirable to produce visible light in order to exploit the high efficiencies of PIN diodes and photomultiplier tubes. Therefore, if highly efficient scintillator neutron detection systems are to be realized using $Li_2B_4O_7$, then the neutron capture must be maximized, as the bandgap is engineered to produce more transitions to a longer wavelength (i.e., in the visible range) while being unaffected by environmental factors such as temperature. One bandgap-engineering option for increasing the wavelength in the light emission spectrum is through the inclusion of defects into the $Li_2B_4O_7$ structure. It has been shown that surface states [68,75] produce photovoltaic charging effects on the material, pinning the surface potential 3.5 eV away from the conduction band minimum (see Figure 3) [76]. Therefore, surfaces states and defects can lead to scintillation in the near-visible [77–79], as shown in Figure 10b.

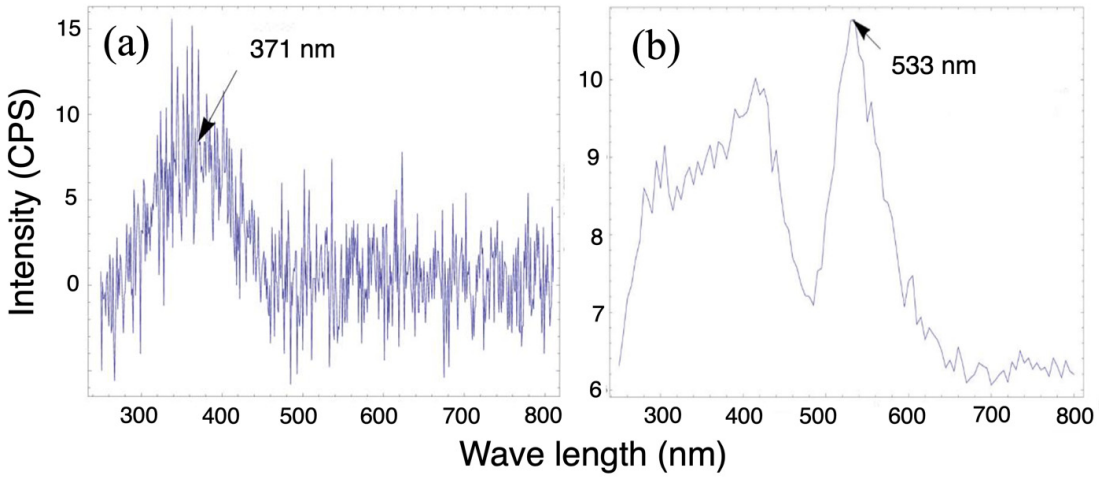

Figure 10. Luminescent response in $Li_2B_4O_7$ to α radiation from ^{241}Am without (**a**) and with (**b**) Ag doping. Luminescent response in $Li_2B_4O_7$ peaks at around 371 nm (**a**) but peaks at 533 nm with (**b**) Ag doping.

Most of the rare earths exhibit emission in the visible region and into the near-infrared region [37,44]. Depending on the host, these transitions can be modified; however, all the electronic levels of the rare earth will remain inside of the bandgap of the host. When the rare earth takes the place of one of the atoms in the host, such sites become a trap center. The new transitions or trap energies can be observed via thermoluminescence, radioluminescence, or light output measurements. In 1996, Wojtowicz [80] used a simple band structure model to study the scintillation mechanism of a compound in the form of AB_3 doped with a rare earth ion and found that, depending on the *f*-*s* energy promotion [80] a rare earth ion will act as an electron or hole trap. Energy calculations, based upon the *f*-*s* transition energy, propose lanthanide ions as the prime candidates to be used as activators for electron or hole traps. These ions can be used in $Li_2B_4O_7$-based compounds (as shown in Figure 11) to act as outstanding activators for modification of the luminescence spectrum [80].

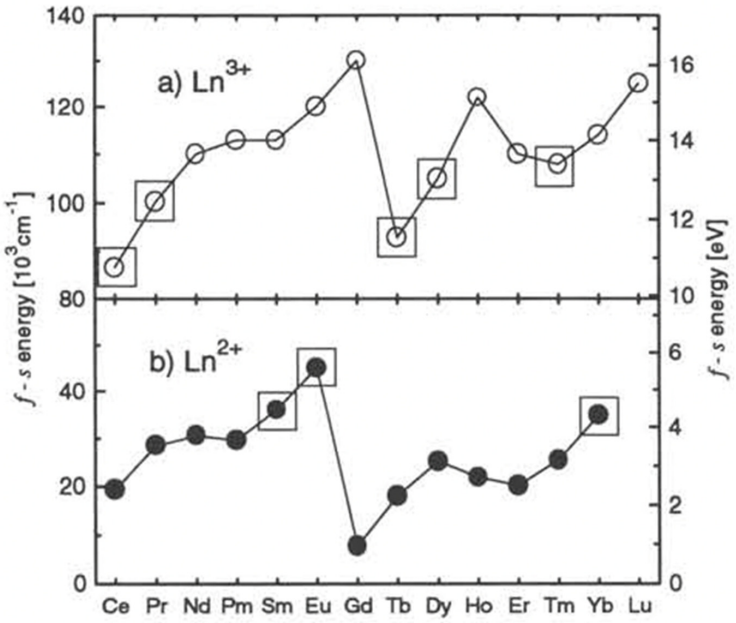

Figure 11. Energies of f-s transition for rare earth (RE = Ln in the figure) ions in their 3+ and 2+ states. The ions most likely to act as an electron (**bottom curve**) or hole (**top curve**) traps are indicated by squares. Adapted from [80].

Not only are the luminescence spectra of rare earth-doped $Li_2B_4O_7$ affected by the kind of rare earth dopant [11,22,24–26,30,32,34,40,41,47,81]; they are also affected by the rare earth dopant's concentration [30,81] and the growth atmosphere [34]. The preliminary work of Zadneprovski et al. [11] suggests that co-doping $Li_2B_4O_7$ with Cu along with many rare earth dopant additions leads to a very efficient neutron scintillation (Figure 12), and this may limit the available concentrations of activators when managing the overall luminescence spectrum.

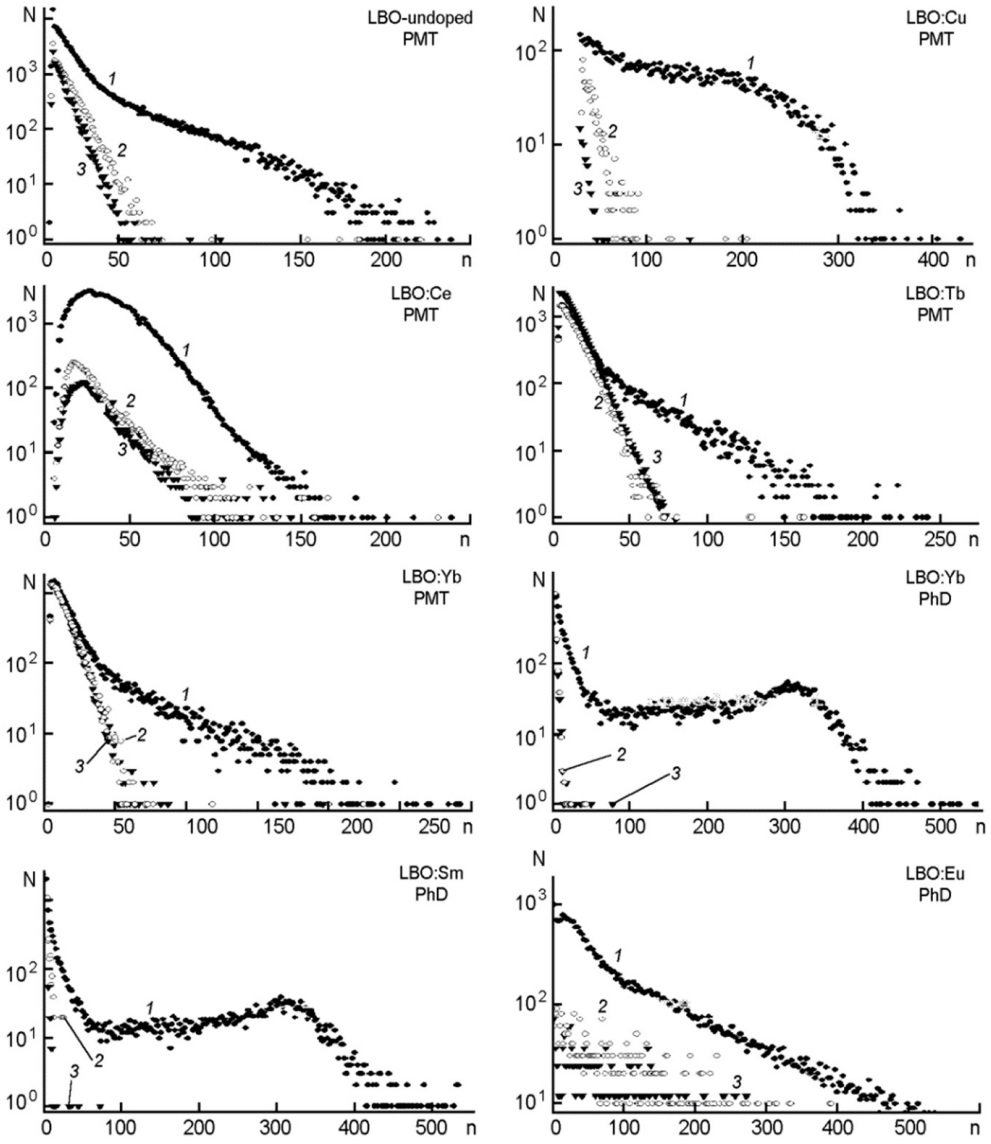

Figure 12. The neutron pulse height spectra (1) taken from a Pu(Be) source (•) compared to γ radiation (2) from a ^{60}Co source (o) and background (3,▼) from various doped and undoped lithium tetraborates. Adapted from [11].

Rare earth elements tend to occupy the Li^+ sites of $Li_2B_4O_7$ [25,40,47], and the structural geometry of rare earth-doped $Li_2B_4O_7$, as shown in Figure 13, does not change significantly with dopants. The occupation of B sites by a rare earth element is quite unlikely owing to the large difference in the ionic radii of B ions and that of the rare earth elements (and the oxygen coordination number of the rare earth). Li^+ substitution is not the only consequence of rare earth doping; a few site distortions and site disorders are present as well, due to the change in the lengths of the bonds between the rare earth and surrounding atoms. X-ray absorption near-edge structure (EXAFS) data have shown that

bond lengths decrease with the increase in atomic number [25]. It is also known that rare earth impurities on $Li_2B_4O_7$ are present in the form of trivalent (RE^{3+}) ions [32,40,47]. Kelly et al. [25], using density functional theory (DFT), show indications of strong hybridization between rare earth states and the $Li_2B_4O_7$ host. In their study [25], they used five rare earth elements: Nd, Gd, Dy, Er, and Yb; however, only the first four demonstrate overlapping of the unoccupied 4f levels of the rare earth with the conduction band of $Li_2B_4O_7$ [25]. This finding is another indication that rare earth elements tend to occupy Li^+ instead of B, because Li^+ is bonded to the B_4O_7 by ionic bonds, while boron and oxygen are strongly tied via covalent bonds. The importance of understanding hybridization in scintillators cannot be emphasized enough because significant hybridization between the rare earth states and the $Li_2B_4O_7$ host can increase luminescence and decrease excited-state lifetimes. The rare earths will add states within the undoped $Li_2B_4O_7$, reducing the bandgap at high concentrations without affecting the transparency [24].

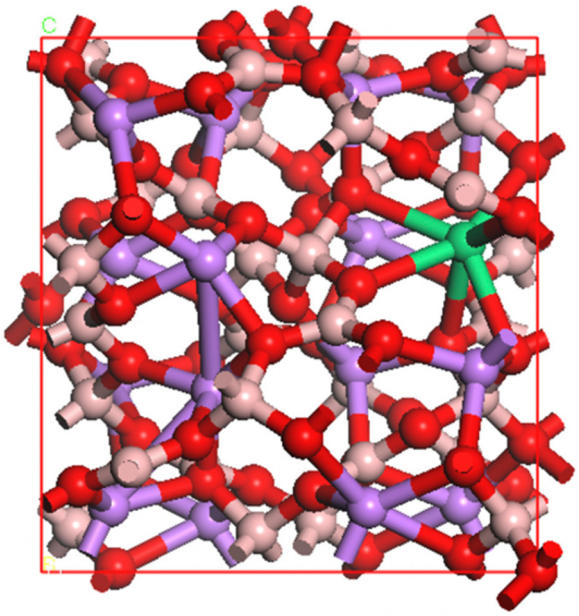

Figure 13. Structural model of the rare earth-doped $Li_{15}B_{32}O_{56}$. Oxygen (red), boron (light pink), lithium (purple), and RE (green). Both the theory and experiment evince that the RE occupies the Li^+ site. Modified from [25].

A final challenge when adding activators to $Li_2B_4O_7$ is in avoiding degradation to transparency. This is still a ripe area for research and material advancement. In experiments involving the doping of $Li_2B_4O_7$ with 3% Er via concentration, photo-optical characterization demonstrated no reduction in transparency; however, little effort has been made to characterize its total scintillation efficiency [25]. Er, like Ce, Eu, Tm, and Yb, is a rare earth element with similar chemical behavior, and, thus, other rare earth elements also appear quite promising.

The preliminary results of Kelly et al. [25] are not too surprising given the prior successes with the rare earth doping of $Li_2B_4O_7$. What is still not known is the range of possible elemental concentrations or combinatory mixtures of co-doping $Li_2B_4O_7$ with Cu along with other rare earth elements, such as Ce, Tb, and Er, and their effects on its optical and mechanical properties. In some cases, the optical transparency was improved, while it stayed unaltered in other cases [11]. Additionally, about 80–85% of the transmission in doped $Li_2B_4O_7$ is revealed to be in the range of 350 nm to 800 nm [11], demonstrating the high optical quality of the pure and doped glasses, which is quite an encouraging result (to say the least).

6. Conclusions

In conclusion, $Li_2B_4O_7$ has several inherent physical, atomic, and nuclear properties that establish it as a promising candidate for a high-efficiency, low-power, robust, low false-positive neutron detection medium. Although the elemental content and structure of $Li_2B_4O_7$, along with the possibilities for ^6Li and ^{10}B isotopic enrichment, render it a great candidate for neutron scintillation detector material, there is still substantial room for improvement in order to attain higher quantum efficiencies. Such a goal can be achieved through a better understanding of the parameters affecting detection efficiencies, improved signal-to-noise ratio, background rejections, and self-moderation of MeV neutrons so as to determine the best moderator combination. The interplay of these factors complicates finding the ideal dopants and their respective doping concentration for producing higher scintillation following interactions with neutrons. As it stands, doping $Li_2B_4O_7$ with either europium, ytterbium, samarium, or copper is especially promising, as existing investigations indicate that they can be readily introduced into its crystal structure, barring a few minor detrimental effects to its luminescence and mechanical qualities. All things considered, it is fair to say that further experimental studies on both the scintillation efficiency and transparency of $Li_2B_4O_7$ are needed.

Author Contributions: Conceptualization, E.E., Y.B., J.A.C.S., P.A.D., C.C.I. and A.D.; methodology, J.M., J.P., K.A.N. and D.S.M.; software, L.W. and W.-N.M.; validation, E.E., Y.B., J.A.C.S., I.T., V.A., J.M., J.P., K.A.N., D.S.M.; formal analysis, E.E., Y.B., J.A.C.S., I.T., V.A., J.M., J.P., K.A.N., P.A.D., L.S., K.S., D.S.M. and A.D.; investigation, E.E., Y.B., J.A.C.S., I.T., V.A., J.M., J.P., K.A.N. and D.S.M.; resources, J.M., J.P., P.A.D., C.C.I., D.S.M., Y.B., V.A., A.D. and W.-N.M.; data curation, L.W., W.-N.M., J.M., Y.B., V.A., I.T., K.A.N., D.S.M., J.P.; writing—original draft preparation, E.E., L.S., K.S., C.C.I., J.A.C.S. and A.D.; writing—review and editing, E.E., J.P., D.S.M., P.A.D., C.C.I. and A.D.; visualization, J.P., W.-N.M., Y.B., J.M. and A.D.; supervision, J.M., J.P., A.D., Y.B., D.S.M. and C.C.I.; project administration, C.C.I., E.E., J.M., A.D. and J.P.; funding acquisition, J.P., J.M., W.-N.M. and P.A.D. All authors have read and agreed to the published version of the manuscript.

Funding: This work was supported by Project PID2020-112507GB-I00, funded by MCIN/AEI/10.13039/501100011033; the National Aeronautics and Space Administration, through grants NNX13AN16A, NNX14AL11A, and NNX15AI09H; the Defense Threat Reduction Agency (Grant No. HDTRA1-14-1-0041); Nebraska Public Power District through the Nebraska Center for Energy Sciences Research; and the National Science Foundation through EPSCoR RII Track-1: Emergent Quantum Materials and Technologies (EQUATE), Award OIA-2044049.

Data Availability Statement: The datasets generated during and/or analyzed during the current study are available from the corresponding authors upon reasonable request.

Acknowledgments: The authors would like to thank Benjamin W. Montag, Brant E. Kananen, and T. D. Kelly for their technical support.

Conflicts of Interest: The authors declare that they have no known competing financial interests or personal relationships that could have appeared to influence the work reported in this article.

References

1. Kouzes, R.T. Detecting Illicit Nuclear Materials: The Installation of Radiological Monitoring Equipment in the United States and Overseas Is Helping Thwart Nuclear Terrorism. *Am. Sci.* **2005**, *93*, 422–427. [CrossRef]
2. Kouzes, R.T.; Ely, J.H.; Erikson, L.E.; Kernan, W.J.; Lintereur, A.T.; Siciliano, E.R.; Stephens, D.L.; Stromswold, D.C.; Van Ginhoven, R.M.; Woodring, M.L. Neutron Detection Alternatives to ^3He for National Security Applications. *Nucl. Instrum. Methods Phys. Res. A* **2010**, *623*, 1035–1045. [CrossRef]
3. Seymour, R.S.; Richardson, B.; Morichi, M.; Bliss, M.; Craig, R.A.; Sunberg, D.S. Scintillating-Glass-Fiber Neutron Sensors, Their Application and Performance for Plutonium Detection and Monitoring. *J. Radioanal. Nucl. Chem.* **2000**, *243*, 387–388. [CrossRef]
4. Van der Ende, B.M.; Li, L.; Godin, D.; Sur, B. Stand-off Nuclear Reactor Monitoring with Neutron Detectors for Safeguards and Non-Proliferation Applications. *Nat. Commun.* **2019**, *10*, 1959. [CrossRef] [PubMed]
5. Eijk, C.W.E. van Inorganic Scintillators in Medical Imaging. *Phys. Med. Biol.* **2002**, *47*, R85–R106. [CrossRef] [PubMed]
6. Bird, K.; Sherwin, M.J. *American Prometheus: The Triumph and Tragedy of J. Robert Oppenheimer*; Alfred A. Knopf: New York, NY, USA, 2005.

7. Caruso, A.N. The Physics of Solid-State Neutron Detector Materials and Geometries. *J. Phys. Condens. Matter* **2010**, *22*, 443201. [CrossRef]
8. Frangville, C.; Grabowski, A.; Dumazert, J.; Montbarbon, E.; Lynde, C.; Coulon, R.; Venerosy, A.; Bertrand, G.H.V.; Hamel, M. Nanoparticles-Loaded Plastic Scintillators for Fast/Thermal Neutrons/Gamma Discrimination: Simulation and Results. *Nucl. Instrum. Methods Phys. Res. A* **2019**, *942*, 162370. [CrossRef]
9. Leo, W.R. *Techniques for Nuclear and Particle Physics Experiments*; Springer: Berlin/Heidelberg, Germany, 1994; ISBN 978-3-540-57280-0.
10. Burak, Y.V.; Adamiv, V.T.; Teslyuk, I.M.; Shevel, V.M. Optical Absorption of Isotopically Enriched $Li_2B_4O_7$ Single Crystals Irradiated by Thermal Neutrons. In *Radiation Measurements*; Pergamon: Bergama, Turkey, 2004; Volume 38, pp. 681–684.
11. Zadneprovski, B.I.; Eremin, N.V.; Paskhalov, A.A. New Inorganic Scintillators on the Basis of LBO Glass for Neutron Detection. *Funct. Mater.* **2005**, *12*, 261–268.
12. Seidl, E.; Schwertführer, W. Lithiumborat-Einkristalle Als Neutronendetektoren. *Atomkernenergie* **1966**, *11*, 155–162.
13. Vinograd, E.L.; Vydai, Y.T.; Zagariy, L.B.; Kosmyna, M.B.; Kudin, A.M.; Levin, A.B.; Nazarenko, B.P.; Tarasov, V.A.; Chernikov, V.V. Scintillation Parameters of Single Crystals Containing Lithium: $Li_2B_4O_7$, $LiTaO_3$, $LiNbO_3$. *Funct. Mater.* **1994**, *1*, 152–154.
14. Bhalla, A.S.; Cross, L.E.; Whatmore, R.W. Pyroelectric and Piezoelectric Properties of Lithium Tetraborate Single Crystal. *Jpn. J. Appl. Phys.* **1985**, *24*, 727. [CrossRef]
15. Adamiv, V.T.; Burak, Y.V.; Wooten, D.J.; McClory, J.; Petrosky, J.; Ketsman, I.; Xiao, J.; Losovyj, Y.B.; Dowben, P.A. The Electronic Structure and Secondary Pyroelectric Properties of Lithium Tetraborate. *Materials* **2010**, *3*, 4550–4579. [CrossRef]
16. Ketsman, I.; Wooten, D.; Xiao, J.; Losovyj, Y.B.; Burak, Y.V.; Adamiv, V.T.; Sokolov, A.; Petrosky, J.; McClory, J.; Dowben, P.A. The Off-Axis Pyroelectric Effect Observed for Lithium Tetraborate. *Phys. Lett. A* **2010**, *374*, 891–895. [CrossRef]
17. Marzouk, Z.G.; Dhingra, A.; Burak, Y.; Adamiv, V.; Teslyuk, I.; Dowben, P.A. Long Carrier Lifetimes in Crystalline Lithium Tetraborate. *Mater. Lett.* **2021**, *297*, 129978. [CrossRef]
18. Wooten, D.; Ketsman, I.; Xiao, J.; Losovyj, Y.B.; Petrosky, J.; McClory, J.; Burak, Y.V.; Adamiv, V.T.; Brown, J.M.; Dowben, P.A. The Electronic Structure of $Li_2B_4O_7$(110) and $Li_2B_4O_7$(100). *EPJ Appl. Phys.* **2010**, *52*, 31601. [CrossRef]
19. Baumer, V.N.; Chernikov, V.V.; Dubovik, M.F.; Gavrylyuk, V.P.; Grinyov, B.V.; Grin, L.A.; Korshikova, T.I.; Shekhovtsov, A.N.; Sysoeva, E.P.; Tolmachev, A.V.; et al. Comparative Analysis of Scintillation Parameters Peculiarities of $Li_2B_4O_7$, LaB_3O_6, $Li_6Gd(BO_3)_3$ Single Crystals. *Funct. Mater.* **2001**, *8*, 736–741.
20. Özdemir, Z.; Özbayoğlu, G.; Yilmaz, A. Investigation of Thermoluminescence Properties of Metal Oxide Doped Lithium Triborate. *J. Mater. Sci.* **2007**, *42*, 8501–8508. [CrossRef]
21. Ogorodnikov, I.N.; Pustovarov, V.A.; Kruzhalov, A.V.; Isaenko, L.I.; Kirm, M.; Zimmerer, G. Self-Trapped Excitons in LiB_3O_5 and $Li_2B_4O_7$ Lithium Borates: Time-Resolved Low-Temperature Luminescence VUV Spectroscopy. *Phys. Solid State* **2000**, *42*, 464–472. [CrossRef]
22. Podgórska, D.; Kaczmarek, S.M.; Drozdowski, W.; Berkowski, M.; Worsztynowicz, A. Growth and Optical Properties of $Li_2B_4O_7$ Single Crystals Pure and Doped with Yb, Co and Mn Ions for Nonlinear Applications. *Acta Phys. Pol. A* **2005**, *107*, 507–518. [CrossRef]
23. Dubovik, M.F.; Tolmachev, A.V.; Grinyov, B.V.; Grin, L.A.; Dolzhenkova, E.F.; Dobrotvorskaya, M.V. Luminescence and Radiation-Induced Defects in $Li_2B_4O_7$:Eu Single Crystals. *Quantum Electron. Optoelectron.* **2000**, *3*, 420–422. [CrossRef]
24. Kindrat, I.I.; Padlyak, B.V.; Lisiecki, R.; Adamiv, V.T. Spectroscopic and Luminescent Properties of the Lithium Tetraborate Glass Co-Doped with Tm and Ag. *J. Lumin.* **2020**, *225*, 117357. [CrossRef]
25. Kelly, T.D.; Petrosky, J.C.; McClory, J.W.; Adamiv, V.T.; Burak, Y.V.; Padlyak, B.V.; Teslyuk, I.M.; Lu, N.; Wang, L.; Mei, W.-N.; et al. Rare Earth Dopant (Nd, Gd, Dy, and Er) Hybridization in Lithium Tetraborate. *Front. Phys.* **2014**, *2*, 31. [CrossRef]
26. Kindrat, I.I.; Padlyak, B.V.; Lisiecki, R.; Adamiv, V.T. Spectroscopic and Luminescent Properties of the Lithium Tetraborate Glass Co-Doped with Nd and Ag. *J. Alloys Compd.* **2021**, *853*, 157321. [CrossRef]
27. Nagirnyi, V.; Kotlov, A.; Corradi, G.; Watterich, A.; Kirm, M. Electronic Transitions in $Li_2B_4O_7$:Cu Single Crystals. *Phys. Status Solidi C* **2007**, *4*, 885–888. [CrossRef]
28. Patra, G.; Singh, A.; Tiwari, B.; Singh, S.; BARe, D.D. Undefined Development of Thermal Neutron Detector Based on Lithium Tetraborate (LTB) Single Crystal. 2015. Available online: barc.gov.in (accessed on 24 November 2023).
29. Chen, Y.; Huang, Y.; Luo, Z. Spectroscopic Properties of Yb^{3+} in Bismuth Borate Glasses. *Chem. Phys. Lett.* **2003**, *382*, 481–488. [CrossRef]
30. Danilyuk, P.S.; Popovich, K.P.; Puga, P.P.; Gomonai, A.I.; Primak, N.V.; Krasilinets, V.N.; Turok, I.I.; Puga, G.D.; Rizak, V.M. Optical Absorption Spectra and Energy Levels of Er^{3+} Ions in Glassy Lithium Tetraborate Matrix. *Opt. Spectrosc.* **2014**, *117*, 759–763. [CrossRef]
31. Ignatovych, M.; Holovey, V.; Watterich, A.; Vidóczy, T.; Baranyai, P.; Kelemen, A.; Chuiko, O. Luminescence Characteristics of Cu- and Eu-Doped $Li_2B_4O_7$. *Radiat. Meas.* **2004**, *38*, 567–570. [CrossRef]
32. Ishii, M.; Kuwano, Y.; Asaba, S.; Asai, T.; Kawamura, M.; Senguttuvan, N.; Hayashi, T.; Koboyashi, M.; Nikl, M.; Hosoya, S.; et al. Luminescence of Doped Lithium Tetraborate Single Crystals and Glass. *Radiat. Meas.* **2004**, *38*, 571–574. [CrossRef]
33. Jayasankar, C.K.; Babu, P. Optical Properties of Sm^{3+} Ions in Lithium Borate and Lithium Fluoroborate Glasses. *J. Alloys Compd.* **2000**, *307*, 82–95. [CrossRef]
34. Kaczmarek, S.M. $Li_2B_4O_7$ Glasses Doped with Cr, Co, Eu and Dy. *Opt. Mater.* **2002**, *19*, 189–194. [CrossRef]

35. Kassab, L.; Tatumi, S.; Morais, A.; Courrol, L.; Wetter, N.; Salvador, V. Spectroscopic Properties of Lead Fluoroborate Glasses Doped with Ytterbium. *Opt. Express* **2001**, *8*, 585. [CrossRef] [PubMed]
36. Kelly, T.D.; Kong, L.; Buchanan, D.A.; Brant, A.T.; Petrosky, J.C.; McClory, J.W.; Adamiv, V.T.; Burak, Y.V.; Dowben, P.A. EXAFS and EPR Analysis of the Local Structure of Mn-Doped $Li_2B_4O_7$. *Phys. Status Solidi B* **2013**, *250*, 1376–1383. [CrossRef]
37. Kenyon, A. Recent Developments in Rare-Earth Doped Materials for Optoelectronics. *Prog. Quantum Electron.* **2002**, *26*, 225–284. [CrossRef]
38. Kobayashi, M.; Ishii, M.; Senguttuvan, N. Scintillation Characteristics of Undoped and Cu^+-Doped $Li_2B_4O_7$ Single Crystals. *arXiv* **2015**, arXiv:1503.03759.
39. Lin, H.; Yang, D.; Liu, G.; Ma, T.; Zhai, B.; An, Q.; Yu, J.; Wang, X.; Liu, X.; Yue-Bun Pun, E. Optical Absorption and Photoluminescence in Sm^{3+}- and Eu^{3+}-Doped Rare-Earth Borate Glasses. *J. Lumin.* **2005**, *113*, 121–128. [CrossRef]
40. Padlyak, B.; Ryba-Romanowski, W.; Lisiecki, R.; Adamiv, V.; Burak, Y.; Teslyuk, I.; Banaszak-Piechowska, A. Optical Spectra and Luminescence Kinetics of the Sm^{3+} and Yb^{3+} Centres in the Lithium Tetraborate Glasses. *Opt. Appl.* **2010**, *40*, 427–438.
41. Padlyak, B.; Ryba-romanowski, W.; Lisiecki, R.; Pieprzyk, B.; Drzewiecki, A.; Adamiv, V.; Burak, Y.; Teslyuk, I. Synthesis and Optical Spectroscopy of the Lithium Tetraborate Glasses, Doped with Terbium and Dysprosium. *Opt. Appl.* **2012**, XLII. [CrossRef]
42. Vivien, D.; Georges, P. Crystal Growth, Optical Spectroscopy and Laser Experiments on New Yb^{3+}-Doped Borates and Silicates. *Opt. Mater.* **2003**, *22*, 81–83. [CrossRef]
43. Polisadova, E.F.; Valiev, D.T.; Belikov, K.N.; Egorova, N.L. Scintillation Lithium-Phosphate-Borate Glasses Doped by REI. *Glass Phys. Chem.* **2015**, *41*, 98–103. [CrossRef]
44. Rivera, V.A.G.; Ferri, F.A.; Marega, E. Localized Surface Plasmon Resonances: Noble Metal Nanoparticle Interaction with Rare-Earth Ions. In *Plasmonics—Principles and Applications*; InTech: Houston, TX, USA, 2012.
45. Shimizugawa, Y.; Umesaki, N.; Qiu, J.; Hirao, K. Local Structure around Europium Ions Doped in Borate Glasses. *J. Synchrotron Radiat.* **1999**, *6*, 624–626. [CrossRef]
46. Pisarski, W.A.; Pisarska, J.; Dominiak-Dzik, G.; Ryba-Romanowski, W. Visible and Infrared Spectroscopy of Pr^{3+} and Tm^{3+} Ions in Lead Borate Glasses. *J. Phys. Condens. Matter* **2004**, *16*, 6171–6184. [CrossRef]
47. Senguttuvan, N.; Ishii, M.; Shimoyama, M.; Kobayashi, M.; Tsutsui, N.; Nikl, M.; Dusek, M.; Shimizu, H.M.; Oku, T.; Adachi, T.; et al. Crystal Growth and Luminescence Properties of $Li_2B_4O_7$ Single Crystals Doped with Ce, In, Ni, Cu and Ti Ions. *Nucl. Instrum. Methods Phys. Res. A* **2002**, *486*, 264–267. [CrossRef]
48. Santos, C.; Lima, A.F.; Lalic, M.V. First-Principles Study of Structural, Electronic, Energetic and Optical Properties of Substitutional Cu Defect in $Li_2B_4O_7$ Scintillator. *J. Alloys Compd.* **2018**, *735*, 756–764. [CrossRef]
49. Rzyski, B.M.; Morato, S.P. Luminescence Studies of Rare Earth Doped Lithium Tetraborate. *Nucl. Instrum. Methods* **1980**, *175*, 62–64. [CrossRef]
50. Saisudha, M.B.; Ramakrishna, J. Effect of Host Glass on the Optical Absorption Properties of Nd^{3+}, Sm^{3+}, and Dy^{3+} in Lead Borate Glasses. *Phys. Rev. B* **1996**, *53*, 6186–6196. [CrossRef]
51. Pekpak, E.; Yilmaz, A.; Ozbayoglu, G. An Overview on Preparation and TL Characterization of Lithium Borates for Dosimetric Use. *Open Miner. Process. J.* **2010**, *3*, 14–24. [CrossRef]
52. Knoll, G.F. *Radiation Detection and Measurement*, 3rd ed.; John Wiley & Sons Inc: New York, NY, USA, 1999.
53. Chaminade, J.P.; Viraphong, O.; Guillen, F.; Fouassier, C.; Czirr, B. Crystal Growth and Optical Properties of New Neutron Detectors Ce^{3+}:$Li_6R(BO_3)_3$ (R = Gd,Y). *IEEE Trans. Nucl. Sci.* **2001**, *48*, 1158–1161. [CrossRef]
54. Chernikov, V.V.; Dubovik, M.F.; Gavrylyuk, V.P.; Grinyov, B.V.; Griǹ, L.A.; Korshikova, T.I.; Shekhovtsov, A.N.; Sysoeva, E.P.; Tolmachev, A.V.; Zelenskaya, O.V. Peculiarities of Scintillation Parameters of Some Complex Composition Borate Single Crystals. *Nucl. Instrum. Methods Phys. Res. A* **2003**, *498*, 424–429. [CrossRef]
55. Ishii, M.; Kuwano, Y.; Asai, T.; Asaba, S.; Kawamura, M.; Senguttuvan, N.; Hayashi, T.; Kobayashi, M.; Nikl, M.; Hosoya, S.; et al. Boron Based Oxide Scintillation Glass for Neutron Detection. *Nucl. Instrum. Methods Phys. Res. A* **2005**, *537*, 282–285. [CrossRef]
56. Burak, Y.V.; Adamiv, V.T.; Teslyuk, I.M.; Antonyak, O.T.; Malynych, S.Z.; Pidzyrailo, M.S. Thermoluminescence in Doped Single Crystals $Li_2B_4O_7$:A (A = Cu, Ag). *Ukrayins'kij Fyizichnij Zhurnal Kiev* **2005**, *50*, 1153–1158.
57. Islam, M.M.; Maslyuk, V.V.; Bredow, T.; Minot, C. Structural and Electronic Properties of $Li_2B_4O_7$. *J. Phys. Chem. B* **2005**, *109*, 13597–13604. [CrossRef] [PubMed]
58. Wooten, D.; Ketsman, I.; Xiao, J.; Losovyj, Y.B.; Petrosky, J.; McClory, J.; Burak, Y.V.; Adamiv, V.T.; Dowben, P.A. The Surface Core Level Shift for Lithium at the Surface of Lithium Borate. *Phys. B Condens. Matter* **2010**, *405*, 461–464. [CrossRef]
59. Sugawara, T.; Komatsu, R.; Uda, S. Linear and Nonlinear Optical Properties of Lithium Tetraborate. *Solid State Commun.* **1998**, *107*, 233–237. [CrossRef]
60. Borlido, P.; Schmidt, J.; Huran, A.W.; Tran, F.; Marques, M.A.L.; Botti, S. Exchange-Correlation Functionals for Band Gaps of Solids: Benchmark, Reparametrization and Machine Learning. *NPJ Comput. Mater.* **2020**, *6*, 96. [CrossRef]
61. Lentz, L.C.; Kolpak, A.M. Predicting HSE Band Gaps from PBE Charge Densities via Neural Network Functionals. *J. Phys. Condens. Matter* **2020**, *32*, 155901. [CrossRef]
62. Perdew, J.P. Density Functional Theory and the Band Gap Problem. *Int. J. Quantum Chem.* **1985**, *28*, 497–523. [CrossRef]
63. Perdew, J.P.; Yang, W.; Burke, K.; Yang, Z.; Gross, E.K.U.; Scheffler, M.; Scuseria, G.E.; Henderson, T.M.; Zhang, I.Y.; Ruzsinszky, A.; et al. Understanding Band Gaps of Solids in Generalized Kohn–Sham Theory. *Proc. Natl. Acad. Sci. USA* **2017**, *114*, 2801–2806. [CrossRef]

64. Rasmussen, A.; Deilmann, T.; Thygesen, K.S. Towards Fully Automated GW Band Structure Calculations: What We Can Learn from 60.000 Self-Energy Evaluations. *NPJ Comput. Mater.* **2021**, *7*, 22. [CrossRef]
65. Kwon, T.Y.; Ju, J.J.; Kim, H.K.; Cha, J.W.; Kim, J.N.; Cha, M.; Yun, S.I. Linear Optical Properties and Characteristics of Critically Phase-Matched Second Harmonic Generation of a $Li_2B_4O_7$ Crystal Grown by the Czochralski Method. *Mater. Lett.* **1996**, *27*, 317–321. [CrossRef]
66. Petrov, V.; Rotermund, F.; Noack, F.; Komatsu, R.; Sugawara, T.; Uda, S. Vacuum Ultraviolet Application of $Li_2B_4O_7$ Crystals: Generation of 100 Fs Pulses down to 170 Nm. *J. Appl. Phys.* **1998**, *84*, 5887–5892. [CrossRef]
67. Burak, Y.V.; Adamiv, V.T.; Teslyuk, I.M.; Moroz, I.Y.; Malynych, S.Z. What Is the True Value of Bulk Band Gap of Lithium Tetraborate Single Crystal? *Phys. Chem. Solid State* **2022**, *23*, 113–119. [CrossRef]
68. Wang, L.; Mei, W.N.; Dowben, P.A. The Surface States of Lithium Tetraborate. *J. Phys. Condens. Matter* **2013**, *25*, 045014. [CrossRef] [PubMed]
69. Antonyak, O.T.; Burak, Y.V.; Lyseiko, I.T.; Pidzyrailo, N.S.; Khapko, Z.A. Luminescence of $Li_2B_4O_7$ Crystals. *Opt. Spectrosc.* **1986**, *61*, 550–553.
70. Wettlaufer, J.S.; Jackson, M.; Elbaum, M. A Geometric Model for Anisotropic Crystal Growth. *J. Phys. A Math. Gen.* **1994**, *27*, 5957–5967. [CrossRef]
71. Moustafa, Y.M.; Hassan, A.K.; El-Damrawi, G.; Yevtushenko, N.G. Structural Properties of V_2O_5:Li_2O:B_2O_3 Glasses Doped with Copper Oxide. *J. Non-Cryst. Solids* **1996**, *194*, 34–40. [CrossRef]
72. Klein, C.A. Bandgap Dependence and Related Features of Radiation Ionization Energies in Semiconductors. *J. Appl. Phys.* **1968**, *39*, 2029–2038. [CrossRef]
73. Bussolati, C.; Fiorentini, A.; Fabri, G. Energy for Electron-Hole Pair Generation in Silicon by Electrons and α Particles. *Phys. Rev.* **1964**, *136*, A1756–A1758. [CrossRef]
74. Emery, F.E.; Rabson, T.A. Average Energy Expended Per Ionized Electron-Hole Pair in Silicon and Germanium as a Function of Temperature. *Phys. Rev.* **1965**, *140*, A2089–A2093. [CrossRef]
75. Wooten, D.; Ketsman, I.; Xiao, J.; Losovyj, Y.B.; Petrosky, J.C.; McClory, J.; Burak, Y.; Adamiv, V.; Dowben, P.A. Differences in the Surface Charging at the (100) and (110) Surfaces of $Li_2B_4O_7$. *MRS Proc.* **2009**, *1164*, 1164-L04-04. [CrossRef]
76. Xiao, J.; Lozova, N.; Losovyj, Y.B.; Wooten, D.; Ketsman, I.; Swinney, M.W.; Petrosky, J.; McClory, J.; Burak, Y.V.; Adamiv, V.T.; et al. Surface Charging at the (100) Surface of Cu Doped and Undoped $Li_2B_4O_7$. *Appl. Surf. Sci.* **2011**, *257*, 3399–3403. [CrossRef]
77. Brant, A.T.; Kananan, B.E.; Murari, M.K.; McClory, J.W.; Petrosky, J.C.; Adamiv, V.T.; Burak, Y.V.; Dowben, P.A.; Halliburton, L.E. Electron and Hole Traps in Ag-Doped Lithium Tetraborate ($Li_2B_4O_7$) Crystals. *J. Appl. Phys.* **2011**, *110*, 093719. [CrossRef]
78. Brant, A.T.; Buchanan, D.A.; McClory, J.W.; Dowben, P.A.; Adamiv, V.T.; Burak, Y.V.; Halliburton, L.E. EPR Identification of Defects Responsible for Thermoluminescence in Cu-Doped Lithium Tetraborate ($Li_2B_4O_7$) Crystals. *J. Lumin.* **2013**, *139*, 125–131. [CrossRef]
79. Swinney, M.W.; McClory, J.W.; Petrosky, J.C.; Yang, S.; Brant, A.T.; Adamiv, V.T.; Burak, Y.V.; Dowben, P.A.; Halliburton, L.E. Identification of Electron and Hole Traps in Lithium Tetraborate ($Li_2B_4O_7$) Crystals: Oxygen Vacancies and Lithium Vacancies. *J. Appl. Phys.* **2010**, *107*, 113715. [CrossRef]
80. Wojtowicz, A.J. Scintillation Mechanism: The Significance of Variable Valence and Electron-Lattice Coupling in RE-Activated Scintillators. In *Proceedings of the SCINT-95, Delft, The Netherlands, 28 August–1 September 1995*; University Press: Delft, The Netherlands, 1996; pp. 95–103.
81. Puga, P.P.; Puga, G.D.; Popovich, K.P.; Kel'man, V.A.; Krasylynec, V.N.; Turok, I.I.; Prymak, M.V.; Danyliuk, P.S. Optical Absorption and X-Ray Luminescence of Glassy Lithium Tetraborate Activated by Terbium Oxide. *Glass Phys. Chem.* **2012**, *38*, 190–195. [CrossRef]